ISSN 1814-4225 (print)
ISSN 2663-2012 (online)

UDC 621.452.3.038.26 **doi: 10.32620/aktt.2026.1.01**

Ruslan TSUKANOV

National Aerospace University «Kharkiv Aviation Institute», Kharkiv, Ukraine

COMPARISON OF VARIOUS TURBULENCE MODELS FOR EJECTOR NOZZLE CFD

*The **subject of this** article is the application of various turbulence models to calculations of thrust-augmenting ejector nozzles for jet engines by computational fluid dynamics (CFD). The **goal** is to justify the selection of the turbulence model in CFD-calculations of thrust-augmenting ejector nozzles. The **tasks** addressed include: searching for and analyzing information sources as for application of different turbulence models in CFD-calculations of thrust-augmenting ejector nozzles; selecting a reliable and complete source of experimental data for digital simulation; constructing an axisymmetric model of the ejector nozzle and three meshes (coarse, medium, and fine); establishing boundary conditions; estimating of uncertainty due to discretization using Grid Convergence Index – GCI; verifying mesh independence; validating the calculation model's accuracy; performing calculations using fourteen turbulence models; determining the accuracy ranking of these turbulence models; and formulating recommendations regarding the application of the turbulence models for these problems. The **methods** employed include: a search of relevant information sources on the Internet and analysis based on operational experience in the aviation sector; the method of computational fluid dynamics; digital calculation of Grid Convergence Index; and errors analysis. The following **results** were obtained: based on the analyzed information sources, it was found that the majority of authors of available studies, devoted to thrust-augmenting ejector nozzle, use different versions of k-ε and k-ω turbulence models. Based on the data from NASA memorandum, a computational model of ejector nozzle was constructed; and its accuracy was validated by three different methods (using GCI, by comparing the static pressure distribution along the nozzle shroud, and by comparing the nozzle integral parameters). This model of ejector nozzle was applied to calculations using fourteen turbulence models. Through comparison with NASA, experimental data and multi-criteria expert analysis of the obtained results, the best three turbulence models yielding the lowest errors (in static pressure distribution along the nozzle shroud, and in calculations of the nozzle integral parameters) were identified. **Conclusions.** The scientific novelty of the results obtained lies in the following: based on a comparison of numerical simulation results of the ejector nozzle using fourteen turbulence models with NASA experimental data, three turbulence models demonstrating the lowest errors rates were identified and recommended for calculating thrust-augmenting ejector nozzles. Thus, turbulence models suitable for the development of a design methodology for thrust-augmenting ejector nozzles for micro-turbojets were identified. The goals and challenges of the following research in this field are outlined.*

Keywords: *gas-turbine engine; thrust augmenting ejector nozzle; thrust augmentation; entrainment ratio; primary nozzle; ejector mixing chamber.*

Introduction

In designing practice of aircraft power plants, a situation often appears, when due to change in aircraft performance or flight conditions, it is necessary to search some ways of engine thrust increase. Problem of thrust increase of small turbojets for Unmanned Aerial Vehicles (UAV) is especially urgent because the same engine can be selected for application in many objects having considerably different use conditions. UAVs use very small turbojet engines, having static thrust below 1000 N at sea level. All these turbojets are usually similar in design: a single-stage centrifugal or diagonal compressor delivering low overall pressure ratio (of up to 4…5), and an uncooled turbine, which has limited inlet temperature (up to 1000 °C) [1]. When not great thrust increase is required, redesigning of engine structure with changes of primary unit sizes can be economically unreasonable. One of technically simple and effective methods of thrust increase without changes of primary unit structure is ejector nozzle application.

A review of studies devoted to investigation of thrust augmenting ejectors intended for gas-turbine engines was presented in the article [2] by the authors of this publication. In the article [3], the early performed review of ejectors was supplement with the analysis of studies on application of gas flow mixer development, additional air intakes of secondary flow, analysis of afterbodies air flow, and ejector application in other fields of engineering.

Creative Commons Attribution
NonCommercial 4.0 International

Computational Fluid Dynamics (CFD) models are being used for ejector nozzle analysis since the second half of 1970-th, when power computers were appeared. Thus, for example W. L. Rushmore et al. (1978) [4] presented 3D finite element computer code to analyze ejector (for VTOL aircraft) and mixers (for turbofans).

Since then, CFD software is continuously improved. Thus in 1990, C. G. Speziale et al. [5] presented critical analysis of two-equation turbulent models (including several versions of k-ε and k-ω models). The authors showed that, the k-ε model has two major problems associated with it: 1) the lack of natural boundary conditions for the dissipation rate (which caused to use a variety of derived boundary conditions that are either asymptotically inconsistent or numerically stiff) and 2) the appearance of higher-order correlations in the balance of terms for the dissipation rate at the wall (which can be a source of substantial inaccuracies and numerical stiffness).

In 1992, J. DeBonis [6] presented results of CFD analysis of rectangular mixer/ejector nozzle for supersonic transport aircraft with the purpose of noise suppression at takeoff mode.

In 2004, E. Jason [7] proposed a calculation method (whose main features are in-house numerical software, axisimmetric statement, k-ω turbulence model) for rocket based combined cycle engine, using two approaches: 1) the subsonic airstream was choked before mixing; 2) the exit pressure was specified. The author presented results of systematic study of various ejector designs using Newton-Raphson method to determine Mach numbers of incoming air and exit flow.

In 2007, Y.-H. Liu [8] presented results of numerical research of 12-lobed exhauster-ejector mixer using 3D-statement (domain of one period of lobed mixer was considered, RNG k-ε turbulence model, tetrahedral elements with sizes of 1 mm near wall and 3…5 mm in other region, turbulence intensity of primary flow was 10 %, of secondary one was 5 %).

In 2010, S. Khalid et al. [9] considered mechanism responsible for secondary flow entrainment and thrust augmentation of a cylindrical shroud ejector of subsonic mixed flow turbofan using 2D axi-symmetric CFD analysis (Fluent 6.1, quad cell type of 6 mm, standard k-ε turbulence model, implicit coupled density-based solver (DBS)).

In 2011, D. Thirumurthy et al. [10] presented results of CFD investigation of ejector nozzle with chevrons and clamshells for supersonic cruise aircraft, using three software: ANSYS Fluent 6.3, ANSYS CFX 12.1, Rolls-Royce HYDRA-CFD (3D-statement; quadrant 90°; 2000000…3560000 cells; turbulent intensity of primary flow was 10 %, of secondary one was 0.1 %; k-ω SST turbulence model; explicit coupled DBS).

In 2015, T. Luginsland [11] for the first time in compressible statement investigated the role of the nozzle-wall thickness and the nozzle length on the vortex breakdown on swirling-jet flows of a rotating nozzle.

In 2019, Z. Hoter et al. [12] presented results of numerical study of a one sided flat mixer ejector nozzle with the purpose to provide enough thrust and reduce noise of supersonic passenger airplane during takeoff (Solidworks Flow Simulation, k-ε turbulence model used).

In 2020, Z. Dong et al. [13] considered ejector mode of rocket-based combined-cycle engine operation (ABSYS Fluent 17.0, RANS, SST-k-ω turbulence model, implicit DBS).

In 2020, H. Huang et al. in article [14] considered integrated ejector nozzle with tertiary door (SR-71-type) under zero flight Mach number and low nozzle pressure ratio (0.9…2.1) using CFD analysis (unfortunately the authors have not specified the turbulence model used).

In 2021, H. Li et al. in article [15] define and compare modes of the over-expanded, fully expanded and under-expanded states for a steam ejector using 2D axisymmetric CFD method (ANSYS Fluent 15.0, k-ε realizable turbulence model with Enhanced Wall Friction (EWF), DBS, turbulence intensity of primary flow was 5 %, of secondary one was 2 %.

In 2022 [16] and in 2023 [17], Z. Li et al. considered flat ejector nozzle (based on SR-71 nozzle) with tertiary door in full-open and open-close position using 3D CFD analysis (ANSYS Fluent, unfortunately the authors have not specified the turbulence model used).

In 2023, Z. Li et al. [18] considered four versions of tertiary air inlets (having sector angle: 30°, 22.5°, 18°, and 15°) for supersonic ejector nozzle of SR-71 airplane using 3D CFD method (ANSYS Fluent, k-ω SST turbulence model, DBS).

In 2024, F. C. Nwoye et al. [19] presented results of CFD investigation of the shear layer interaction, mixing, and entrainment behavior of an ejector design for the different streamlined profiles of the nozzle (ANSYS Fluent, k-ε realizable turbulence model, pressure-based solver (PBS)).

In 2024, A. Vinz et al. [20] presented results of 3D CFD investigations of boundary layer ingestion engine integration concept aimed at modeling and evaluating the inhomogeneous inflow into turbofans positioned on either side of the rear fuselage in order to understand the relationship between degree of embedding and total aircraft thrust requirement (DLR TAU code, 3D, Spalart-Allmaras turbulence model, implicit Euler method in conjunction with LUSGS method).

In 2024, Y. He et al. [21] considered numerical simulation of axisymmetric ejector nozzle integrated with the afterbody of an aircraft, using axisymmetric 2D-model (Fluent 6.3, DBS, k-ω SST turbulence model).

In 2025, S. A. I. Bellary et al. [22] presented re-

ISSN 1814-4225 (print)
ISSN 2663-2012 (online)

sults of 2D CFD investigation of the pressure rise characteristics of a shock train contained within a C-D nozzle representative of a supersonic combustion ramjet (ANSYS, k-ε realizable turbulence model, DBS).

In 2025, G. Scarlatella et al. [23] presented results of 2D CFD and experimental investigation of advanced nozzle concepts for retro-propulsion for vertical take-off vertical landing reusable launch vehicles (ANSYS Fluent 2022R1, k–ω SST turbulence model, PBS).

It is clear from this brief review that in spite of availability of lots of turbulence models, majority of authors used for flow simulation inside ejector nozzles various modifications of two models, namely k-ε (six publications from the considered ones) and k-ω (also six publications). Although, there are a lot of other turbulence models, they are not used for solving this problem. This indicates insufficiency of corresponding researches and arbitrariness of choice of these turbulence models by the authors. Thus, the **goal of this work** is stated as comparison of various turbulence models and justification of choice those, which are the most adequate for gas flow simulation within an ejector nozzle.

1. Problem Statement

1.1. Physical Model

For the research of turbulence model influence on the results of numerical simulation, the nozzle, which is presented in NASA technical memorandum [24], was selected (which contains results of probably the most extensive experiments of 28 configurations of ejector nozzles, complete information about geometry, experimental static pressure distribution along the shroud of nozzles and their integral parameters and distinguishes with reliable data). Although this memorandum was aimed at characteristic investigation of thrust-vectored axisymmetric ejector nozzles, it also contains 10 configurations of unvectored nozzles. Among these 10 configurations, the configuration 9 was chosen, which corresponds to the highest ejector area ratio to primary nozzle throat area (0.62). Further, the regime was selected for simulation, which corresponds the highest corrected secondary-to-primary weight-flow ratio $\omega\sqrt{\tau} = \frac{\dot{m}_s}{\dot{m}_p}\sqrt{\frac{T_{0s}}{T_{0p}}} = 0.21$ and minimal primary nozzle pressure ratio $NPR = 3.0$, that is closer than others to an aircraft subsonic flight mode.

As one can see, the ejector nozzle consists of three parts (Fig. 1, a): outer cylinder, primary nozzle and shroud. Due to presence in [24] of detailed information about sizes of the nozzle elements, the sketch was plotted using KOMPAS-3D v.19 with all sizes transfer from inches to millimeters (Fig. 2).

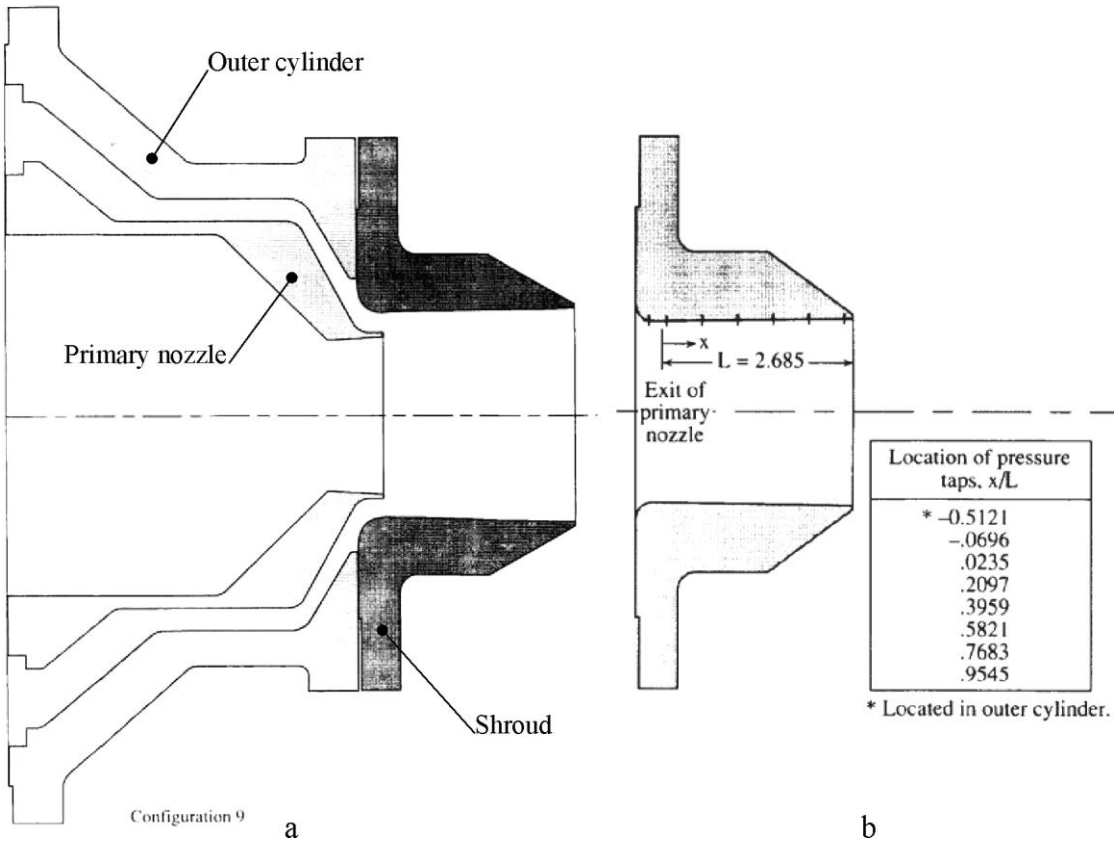

Fig. 1. Configuration 9 of ejector nozzle (a) and locations of pressure sensors in its shroud (b) [24]

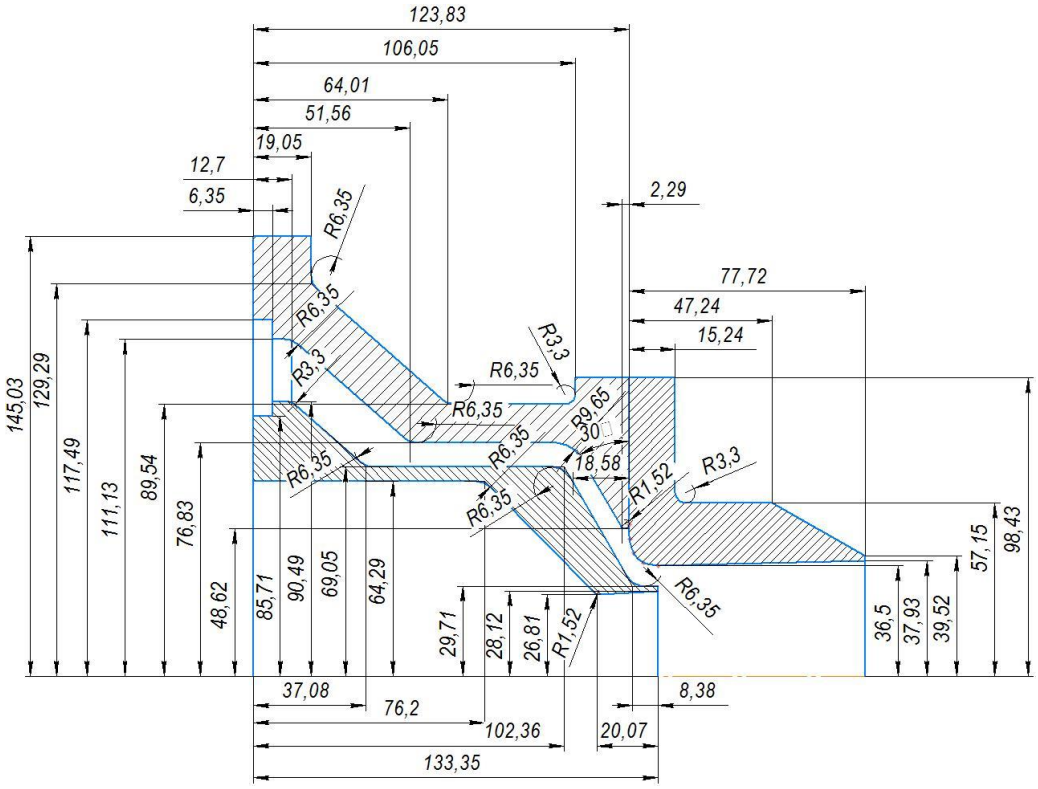

Fig. 2. Sketch of configuration 9 of ejector nozzle in KOMPAS-3D v.19

1.2. Meshing Method

The ejector nozzle considered in this study is axisymmetric, so 2D axisymmetric statement was used, to save calculation time. To specify boundary conditions at «infinite» distance far from the nozzle, the computational domain is large enough with a length of about 10L (2000 mm) in the airflow direction, and a radius of about 2.4R (350 mm), where L=201.55 mm is the total length of the nozzle, and R=145.03 mm is the middle radius of the nozzle (Fig. 3).

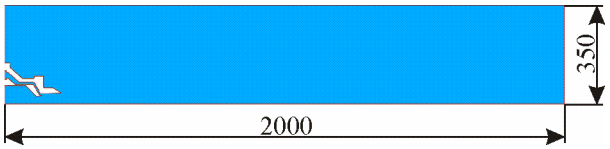

Fig. 3. Computational domain

Standard ANSYS Meshing software was used for mesh generation. Three unstructured meshes were used for mesh independence study, with quadriteral element size equals to 25, 12, and 6 mm. In addition, each mesh near all the nozzle walls was improved by setting Insert\Sizing\Element Size equals to 0.5, 0.25, and 0.12 mm correspondingly (Fig. 4).

1.3. Boundary Conditions and Solution Methods

Figure 5 shows the boundary types of the ejector nozzle model. The free incoming flow, the top, and the right boundaries were adopted as the pressure-outlet boundary type (an attempt to use the pressure-far-field boundary type with zero incoming flow Mach number resulted in ANSYS Fluent crash during hybrid initialization). All the nozzle surfaces were set as nonslip insulating wall.

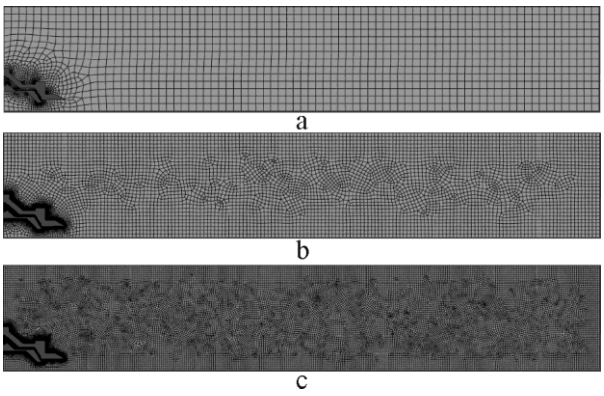

Fig. 4. Three meshes: a – 25 mm; b – 12 mm; c – 6 mm

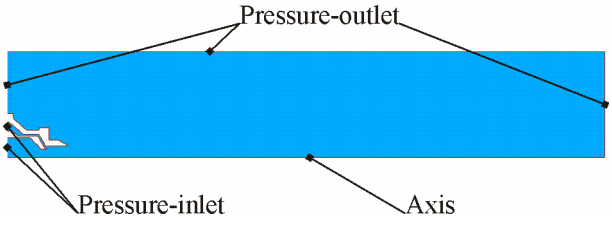

Fig. 5. Boundary types of ejector nozzle model

ISSN 1814-4225 (print)
ISSN 2663-2012 (online)

The nozzle primary and secondary inlets were adopted as the pressure-inlet boundary type. For the simulation, the gauge total pressure, total temperature, turbulent intensity, and hydraulic diameter were specified. The values of the corresponding boundary parameters are listed in Table 1. Actually, the incoming flow Mach number was 0, ambient pressure was $p_0 = 101325$ Pa, and ambient temperature was 288.15 K. The primary nozzle pressure ratio was 3.0, and the secondary nozzle pressure ratio was 1.118. The total temperature of the primary flow was 300.0 K, and the total temperature of the secondary flow was 294.44 K according to [24].

ANSYS Fluent 2024R1 software was used for the numerical simulation. Pressure-Based Solver was used (attempts to use Density-Based Solver resulted in divergence in ANSYS Fluent). k-ε realizable turbulence model with Near-Wall Treatment\Scalable Wall Functions was used for mesh independence calculation (further some turbulence models were compared). Air (ideal-gas, which viscosity was calculated by Sutherland three-coefficient method) was used as fluid. Coupled scheme of the solver was applied together with second order upwind scheme for all equations. In addition, residuals were set to 0.0001. Finally, hybrid initialization was used.

Table 1

Values of corresponding boundary parameters

Boundary\ Parameter	Total pressure, atm	Turbulent intensity, %	Hydraulic diameter, mm	Total temperature, K
Primary inlet	3.000	10	128.58	300.00
Secondary inlet	1.118	1	63.16	294.44
Left, Top	1.000	1	409.94	288.15
Right	1.000	1	700.00	288.15

2. Model Verification and Validation

2.1. Estimation of Uncertainty Due to Discretization

In [25] long established procedure for estimation of discretization error (using Grid Convergence Index – GCI) was proposed, and in [26] the procedure was detailed. Just this procedure is used further.

As it was mentioned beforehand, for mesh independence verification, three meshes were generated, with element size of 25 mm, 12 mm, and 6 mm, which are defined as coarse mesh (index 3), medium mesh (index 2), and fine mesh (index 1) correspondingly.

Step 1. Calculation of the mesh refinement. Using ANSYS Fluent software, we have got representative mesh cell size for coarse, medium, and fine mesh as

$$h = \left[\frac{1}{N} \sum_{i=1}^{N} (\Delta A_i) \right]^{1/2},$$

where N is the total number of cells used for computations; ΔA_i is the area of the i-th cell (denoted as 2D_cell_volume in ANSYS Fluent).

So, they are, m:

$$h_1 = 9.402 \cdot 10^{-6};\ h_2 = 1.422 \cdot 10^{-5};\ h_3 = 5.488 \cdot 10^{-5},$$

corresponding decrease in mean cell sizes relative specified ones is caused by cell reducing near nozzle solid walls.

Thus the refinement ratio from the coarse to medium mesh is

$$r_{32} = h_3 / h_2 = 3.860,$$

the refinement ratio from the medium to fine mesh is

$$r_{21} = h_2 / h_1 = 1.512.$$

Step 2. Calculation of the observed order of approximation. It is performed be means of iterative solving the following equation with respect to p:

$$p = \frac{1}{\ln(r_{21})} \left| \ln\left| \frac{\phi_3 - \phi_2}{\phi_2 - \phi_1} \right| + \ln\left| \frac{r_{21}^p - s}{r_{32}^p - s} \right| \right|, \qquad (1)$$

where ϕ_i is a key variable important to the objective of simulation study; $s = \operatorname{sign} \frac{\phi_3 - \phi_2}{\phi_2 - \phi_1}$. We adopt the nozzle thrust as this variable:

$$\phi = \dot{m}_{total}(v_{av} - v_0) + A_e(p_{av} - p_0),$$

where $\dot{m}_{total}$ is the total mass flow via ejector nozzle; v_{av} is the average gas velocity at the ejector nozzle exit; v_0 is the average air speed at the left boundary (it is approximately equal to zero); A_e is the shroud exit area; p_{av} is the average static pressure at the ejector nozzle exit; p_0 is the atmospheric pressure (101325 Pa).

From ANSYS Fluent calculations, we have got, N:

$$\phi_1 = 624.710;\ \phi_2 = 620.955;\ \phi_3 = 607.385.$$

Solving the equation (1) in MathCAD, we get:

$$p = 0.882.$$

So, the observed order of approximation is lower than the specified one (second order scheme was used). It can be explained, firstly, by application of unstructured mesh, using these calculations for which is not correct (however, they are widely used) [26], secondly, by limited resources of the used computer (which caused rather big sizes of mesh cells). In addition, as it was stated in [25]: «The agreement of the observed apparent order with the formal order of the scheme used can be taken as a good indication of the grids being in the asymptotic range; the converse should not necessarily be taken as a sign of unsatisfactory calculations».

Step 3. Calculation of the convergence condition. The convergence ratio is calculated as:

$$CR = \frac{\phi_2 - \phi_1}{\phi_3 - \phi_2} = 0.277,$$

when $CR < -1$, it is oscillatory divergence; when $CR \in [-1; 0)$, it is oscillatory convergence; when $CR \in [0; 1)$, it is monotonic convergence; when $CR \geq 1$ it is monotonic divergence.

Thus, according to this procedure, monotonic convergence is observed.

Step 4. Calculation of the Richadrson extrapolation value. It is calculated by the following formula:

$$\phi_{ex} = \frac{r_{21}^p \phi_1 - \phi_2}{r_{21}^p - 1} = 633.241 \text{ N},$$

but it is only expected to work well for cases of monotonic convergence.

Step 5. Calculation of the differences. Error from the coarse to medium mesh:

$$\varepsilon_{32} = \left| \frac{\phi_2 - \phi_3}{\phi_2} \right| = 0.02185 = 2.185 \text{ %};$$

error from the medium to the fine mesh:

$$\varepsilon_{21} = \left| \frac{\phi_1 - \phi_1}{\phi_1} \right| = 0.00601 = 0.601 \text{ %}.$$

Step 6. Calculation of the GCI. GCI for the coarse to medium mesh:

$$GCI_{32} = \frac{1.25\varepsilon_{32}}{r_{32}^p - 1} = 0.01192 = 1.192 \text{ %};$$

GCI for the medium to fine mesh:

$$GCI_{21} = \frac{1.25\varepsilon_{21}}{r_{21}^p - 1} = 0.01707 = 1.707 \text{ %},$$

which should not exceed $(5...10)$ % for parametric studies and $(1...5)$ % for detailed studies.

Thus, GCI values show the accuracy, which is enough even for detailed calculations.

2.2. Verification of Mesh Independence

Distribution of static pressure ratio to the primary flow total pressure ($p_{0p} = 303975$ Pa) along the inner wall of the ejector nozzle shroud (Fig. 6), from the numerical simulation results of these three mesh models are shown in Fig. 7 (origin of x coordinate and locations of pressure sensors were shown in Fig. 1, b). It can be seen that the results obtained by the coarse and medium mesh calculations are very close, with an error of less than 4.8 %; results obtained by the medium and fine mesh calculations are also very close, with an error of less than 1.6 %. So that when the size of mesh cells decreases from coarse to fine, the simulation results are basically independent of the mesh size. Therefore, medium mesh is used in the following calculations.

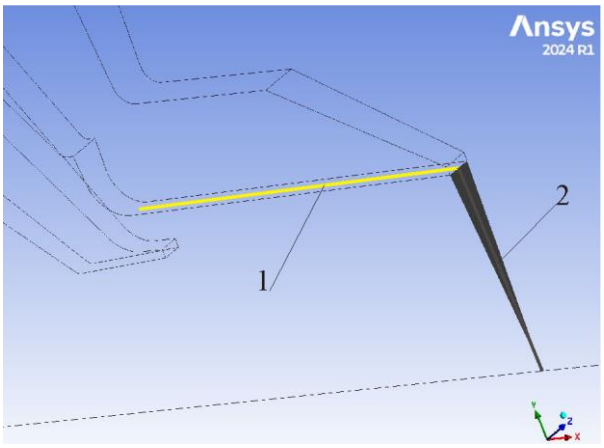

Fig. 6. Line (1) for static pressure distribution along the inner wall of the ejector nozzle shroud and element (2) of shroud exit area

2.3. Experimental Validation

Fig. 7 together with the static pressure distribution along the inner wall of ejector nozzle shroud, obtained by numerical simulation in this study, also shows the pressure distribution according to results of NASA experiments [24]. Excepting the first point (where the difference makes 0.7...4.1 %), the difference between calculated and experimental values does not exceed 1.4 % for coarse mesh; 1.1 % for medium mesh, and 0.9 % for fine mesh.

ISSN 1814-4225 (print)
ISSN 2663-2012 (online)

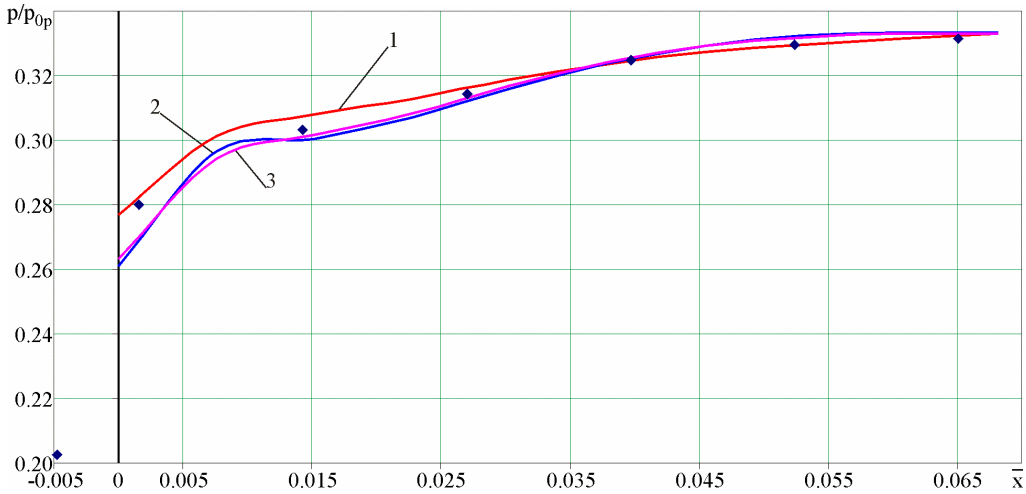

Fig. 7. Comparison of static pressure distribution along the inner wall of ejector nozzle shroud for three different meshes with experimental data: points – NASA experiment [24]; 1 – coarse mesh (element size=25 mm); 2 – medium mesh (element size=12 mm); 3 – fine mesh (element size=6 mm)

In the work [24], there given experimental values of primary nozzle flow coefficient (0.9238) and the ejector nozzle relative thrust (0.9640). The primary nozzle flow coefficient is a ratio of measured flow rate to ideal one. We use formula from work [21] for ideal flow rate via C-D nozzle:

$$\dot{m}_{ip} = p_{0p} A_{thp} \frac{k\sqrt{\left(\frac{2}{k+1}\right)^{\frac{k+1}{k-1}}}}{\sqrt{kRT_{0p}}},$$

where p_{0p} is the primary flow total pressure ($NPR \cdot p_0 = 3.0 \cdot 101325 = 303975$ Pa); A_{thp} is the primary nozzle throat area ($\pi R_{thp}^2 = \pi\left(26.81 \cdot 10^{-3}\right)^2 = 0.002$ mm^2); k is the ratio of specific heats (1.4 for air); R is the gas constant ($R = 287$ J/(kg·K) for air); T_{0p} is the primary flow total temperature.

As the primary flow total temperature is not known from the experiment, it is assumed equal to its static temperature ($T_{0p} \approx T_p = 540$ R $= 300$ K). Thus, the ideal flow rate via the primary nozzle makes $\dot{m}_{ip} = 1.602$ kg/s. Multiplying it by the experimental value of the flow coefficient for this mode, we get experimental value of the primary flow rate:

$$\dot{m}_{ex.p} = 0.9238 \cdot 1.602 = 1.480 \text{ kg/s}.$$

Then (assuming the total temperatures of the both flows equal), the secondary flow rate equals

$$\dot{m}_{ex.s} = \dot{m}_{ex.p} \omega \sqrt{\tau} = 0.311 \text{ kg/s},$$

and the total flow rate via the ejector nozzle

$$\dot{m}_{ex} = \dot{m}_{ex.p} + \dot{m}_{ex.s} = 1.791 \text{ kg/s}.$$

In the work [24], ejector nozzle ideal thrust is calculated as a sum of ideal thrusts of the primary (F_{ip}) and the secondary (F_{is}) flows ($F_i = F_{ip} + F_{is}$), each of them is calculated by the formula:

$$F_{ij} = \dot{m}_j \sqrt{RT_{0j} \frac{2k}{k-1}\left[1 - \left(\frac{1}{NPR_j}\right)^{\frac{k-1}{k}}\right]},$$

where j means the primary or the secondary flows (experimental value of the secondary nozzle pressure ratio makes 1.118).

From these formulas, we get, N:

$$F_{ip} = 602.64; \quad F_{is} = 42.34; \quad F_i = 644.97.$$

Multiplying the experimental value of ejector nozzle relative thrust by this ideal thrust, we get experimental value of the ejector nozzle thrust:

$$F_{ex} = 0.9640 F_i = 621.76 \text{ N}.$$

Dividing this trust by the total flow rate via the ejector nozzle, we get experimental value of average flow speed at the ejector nozzle exit:

$$v_{ex.av} = F_{ex} / \dot{m}_{ex} = 347.261 \text{ m/s}.$$

It is clear from the Table 2 that mistakes of calculations by ANSYS Fluent 2024R1 of the ejector nozzle thrust (Δ_F) does not exceed 2.4 %, of the average flow

Table 2

Mistakes of ejector nozzle parameter calculations

Calculation\Parameter	Δ_F, %	Δ_v, %	Δ_m, %
Mesh 25 mm	2.31	1.60	-0.42
Mesh 12 mm	0.13	-0.82	-0.48
Mesh 6 mm	-0.48	-0.08	-0.22

speed at the ejector nozzle exit (Δ_v) does not exceed 1.6 %, and of the primary flow rate (Δ_m) does not exceed 0.5 % of their experimental values.

Thus, the numerical calculation results showed good agreement with the experimental results; and it is possible to assume that the simulation method used in this study accurately enough simulates the internal flow characteristics of the ejector nozzle.

3. Results and Discussion

Thus, the medium mesh (having element size of 12 mm and improvement near walls to 0.25 mm) was used for the following calculations. In addition after initial calculation (1000 iterations, even in case of no convergence), adaptive mesh was applied, which allowed decreasing of element size just in zones, where high parameter gradients were located. Next, the calculation continued (in case the convergence has already been achieved during initial calculation, the residual for continuity equation was set 10 times less than it was before).

3.1. Comparison of static pressure distribution

Calculations with the same parameters using different turbulence models have been performed. Fig. 8 shows charts of static pressure distribution along the inner wall of ejector nozzle shroud for different turbulence models.

Table 3 shows roof-mean-square deviations and maximum ones of these numerical calculation results from experimental points NASA [24]. «Accuracy priority» values show priority, with which there is a sense to use these turbulence models for ejector nozzle calculations.

Fig. 9 shows the same charts for five turbulence models having the highest priority.

3.2. Comparison of ejector nozzle parameters

Table 4 shows comparison of results of ejector nozzle parameters calculations in ANSYS Fluent 2024R1 for considered turbulence models with experimental values [24].

It is clear from the Table 4 that mistakes of ejector nozzle thrust (Δ_F) calculations do not exceed 1 % for the majority of the considered model. The following models give greater mistake: k-ε (Standard) – 6.77 %; Reynolds-Stress (Stress-Omega) – 1.95 %; and Reynolds-Stress (Stress-BSL) – 1.50 %.

Mistakes of average flow speed at the ejector nozzle exit (Δ_v) calculations for the majority of the considered models do not exceed 5 % (excepting model Reynolds-Stress (Stress-Omega), for which the mistake is 6.94 %).

Mistakes of primary flow rate (Δ_m) calculations for the majority of the considered models do not exceed 1 % (excepting model k-ε (Standard), for which the mistake is 1.67 %).

Table 3

Mistakes of pressure distribution calculations

Turbulence model	Roof-mean-square deviations, %	Accuracy priority	Maximal deviations, %	Accuracy priority
Spalart-Allmaras (Vorticity-Based)	3.46	8	3.24	8
Spalart-Allmaras (Strain/Vorticity-Based)	2.82	7	2.64	7
k-ε (Standard)	56.80	14	37.49	14
k-ε (RNG)	4.05	10	3.57	10
k-ε (Realizable)	3.96	9	3.49	9
k-ω (Standard)	2.77	6	1.68	6
k-ω (GEKO)	1.73	2	1.11	2
k-ω (BSL)	1.30	1	1.01	1
k-ω (SST)	2.02	5	1.32	4
Transition k-kl-ω	14.40	13	10.66	13
Transition SST	1.90	4	1.25	3
Reynolds-Stress (Linear Pressure-Strain)	1.85	3	1.40	5
Reynolds-Stress (Stress-Omega)	7.33	12	6.98	11
Reynolds-Stress (Stress-BSL)	7.24	11	7.06	12

ISSN 1814-4225 (print)
ISSN 2663-2012 (online)

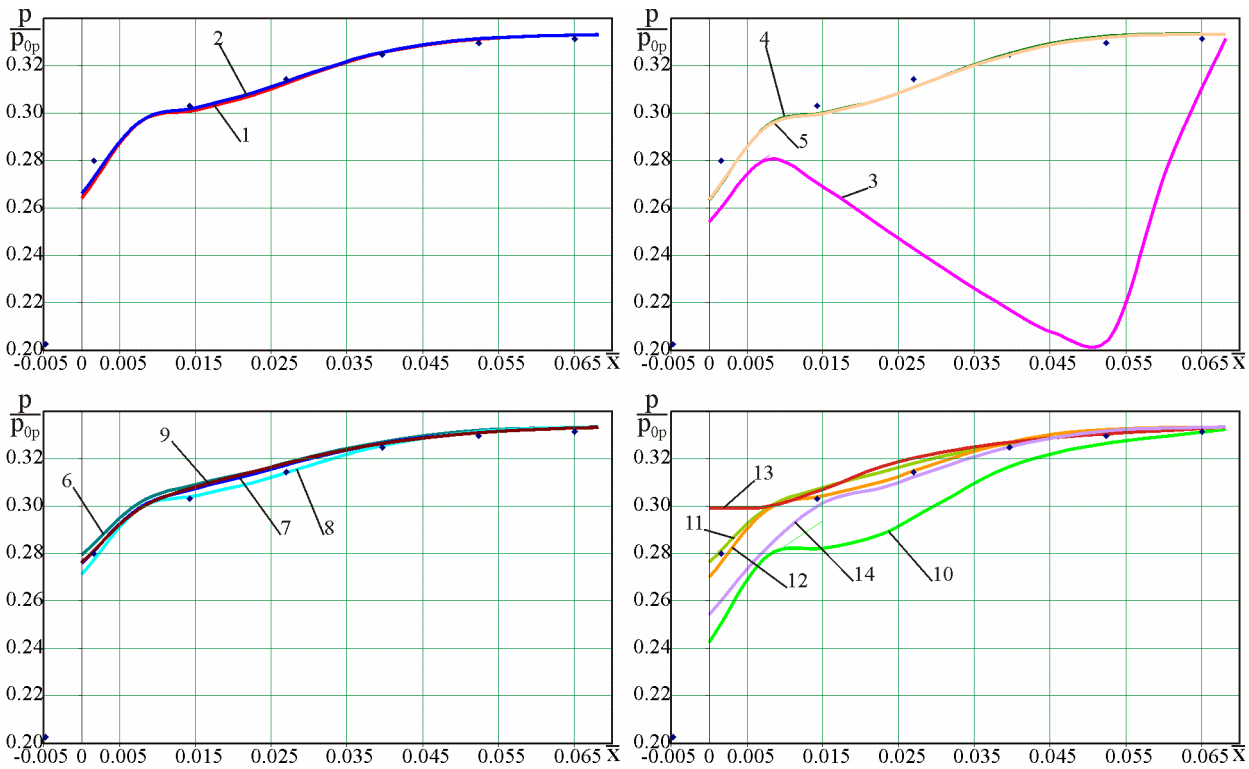

Fig. 8. Comparison of static pressure distribution along the inner wall of ejector nozzle shroud for different turbulence models: points – NASA experiment [24]; 1 – Spalart-Allmaras (Vorticity-Based); 2 – Spalart-Allmaras (Strain/Vorticity-Based); 3 – k-ε (Standard); 4 – k-ε (RNG); 5 – k-ε (Realizable); 6 – k-ω (Standard); 7 – k-ω (GEKO); 8 – k-ω (BSL); 9 – k-ω (SST); 10 – Transition k-kl-ω; 11 – Transition SST; 12 – Reynolds-Stress (Linear Pressure-Strain); 13 – Reynolds-Stress (Stress-Omega); 14 – Reynolds-Stress (Stress-BSL)

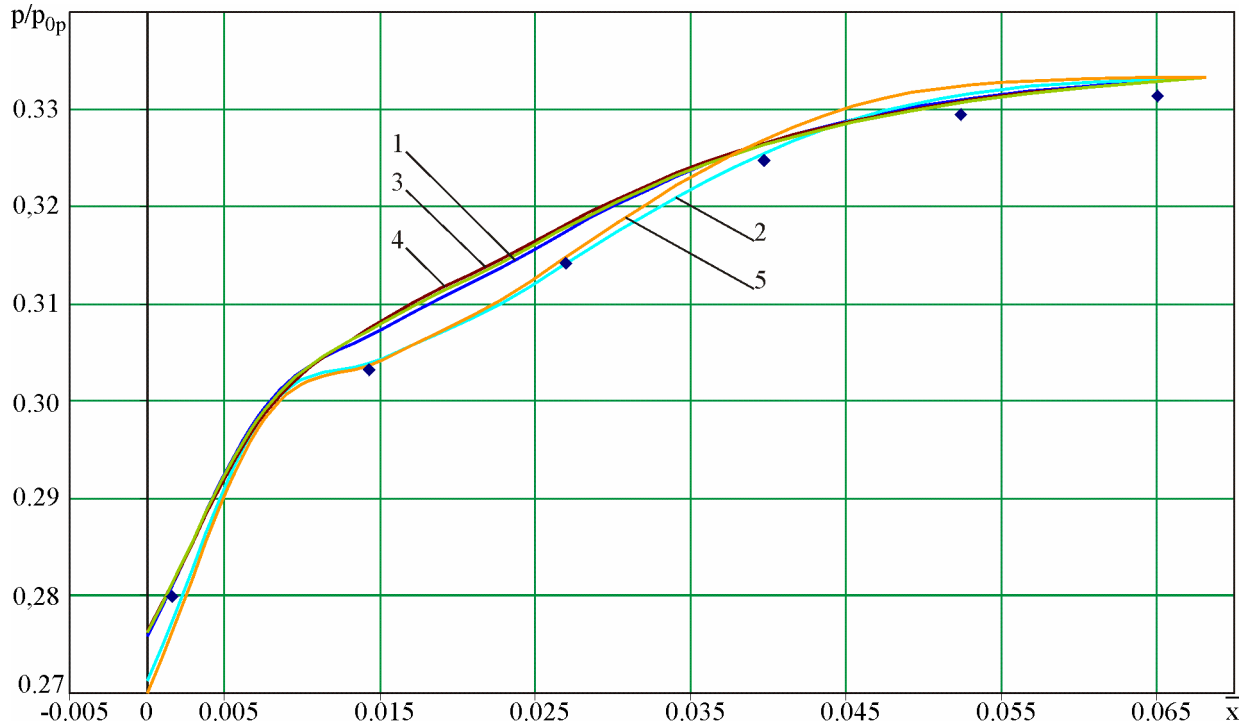

Fig. 9. Comparison of static pressure distribution along the inner wall of ejector nozzle shroud for different turbulence models: points – NASA experiment [24]; 1 – k-ω (GEKO); 2 – k-ω (BSL); 3 – k-ω (SST); 4 – Transition SST; 5 – Reynolds-Stress (Linear Pressure-Strain)

Table 4

Mistakes of ejector nozzle parameters calculations

Model\Parameter	Δ_F, %	Δ_v, %	Δ_m, %
Spalart-Allmaras (Vorticity-Based)	0.52	-3.06	-0.14
Spalart-Allmaras (Strain/Vorticity-Based)	0.49	-3.22	-0.14
k-ε (Standard)	6.77	2.93	-1.67
k-ε (RNG)	0.30	-3.11	-0.04
k-ε (Realizable)	0.21	-2.52	-0.07
k-ω (Standard)	0.98	-3.19	-0.36
k-ω (GEKO)	0.65	-4.32	-0.06
k-ω (BSL)	0.93	-2.36	-0.37
k-ω (SST)	0.72	-4.54	-0.09
Transition k-kl-ω	0.86	-0.70	-0.09
Transition SST	0.65	-4.54	-0.07
Reynolds-Stress (Linear Pressure-Strain)	0.85	-3.62	-0.19
Reynolds-Stress (Stress-Omega)	1.95	-6.94	-0.15
Reynolds-Stress (Stress-BSL)	1.50	-3.62	-0.15

Table 5

Priority analysis

Model	Priorities				
	By pressure	By thrust	By speed	By flow rate	General
Spalart-Allmaras (Vorticity-Based)	3	1	2	1	7
Spalart-Allmaras (Strain/Vorticity-Based)	**2**	**1**	**2**	**1**	**6**
k-ε (Standard)	5	2	2	3	12
k-ε (RNG)	3	1	2	1	7
k-ε (Realizable)	3	1	2	1	7
k-ω (Standard)	2	2	2	1	7
k-ω (GEKO)	1	1	4	1	7
k-ω (BSL)	**1**	**2**	**2**	**1**	**6**
k-ω (SST)	**1**	**1**	**3**	**1**	**6**
Transition k-kl-ω	5	2	1	1	9
Transition SST	1	1	4	1	7
Reynolds-Stress (Linear Pressure-Strain)	1	2	3	1	7
Reynolds-Stress (Stress-Omega)	4	3	5	1	13
Reynolds-Stress (Stress-BSL)	4	3	2	1	10

It is easy to see that the same models, which give the highest mistake of ejector nozzle parameter calculations, are distinguished with the highest mistake of static pressure calculation (see Table 3). Results, obtained by transition k-kl-ω model looks strange enough: it gives very high mistakes of static pressure calculation and very low mistakes of ejector nozzle parameter calculations.

All five the best models by static pressure calculation (k-ω (GEKO); k-ω (BSL); k-ω (SST); Transition SST; Reynolds-Stress (Linear Pressure-Strain)) give

ISSN 1814-4225 (print)
ISSN 2663-2012 (online)

mistakes of ejector nozzle thrust (Δ_F) and primary flow rate (Δ_m) calculation less than 1 %, and mistake of average flow speed at the ejector nozzle exit (Δ_v) calculation, which does not exceed 5 %.

For more objective comparative analysis of turbulence models, one of the simplest types of multicriterion choice on the base of expert judgments [27] can be used. Let's introduce four levels (priorities) of subjective estimation of turbulence model applicability: 1 – the best; 2 – quite applicable; 3 – moderately applicable; 4 – undesirable; 5 – not-applicable. Within the Table 5, corresponding model estimations by separate indexes, and also general estimation, obtained as a sum of the levels, are shown (all the separate indexes were taken with equal weighting coefficients).

Thus, any turbulence model from those, which are marked within the Table 5 with semi-bold font, can be assumed for the following research.

3.3. Fields of Mach number and static pressure inside the ejector nozzle

Fig. 10, a shows field of Mach number, and Fig. 10, b shows field of static pressure inside the considered ejector nozzle for one of the best k-ω (SST) turbulence model, which obtained the highest priorities by three indexes of the four ones.

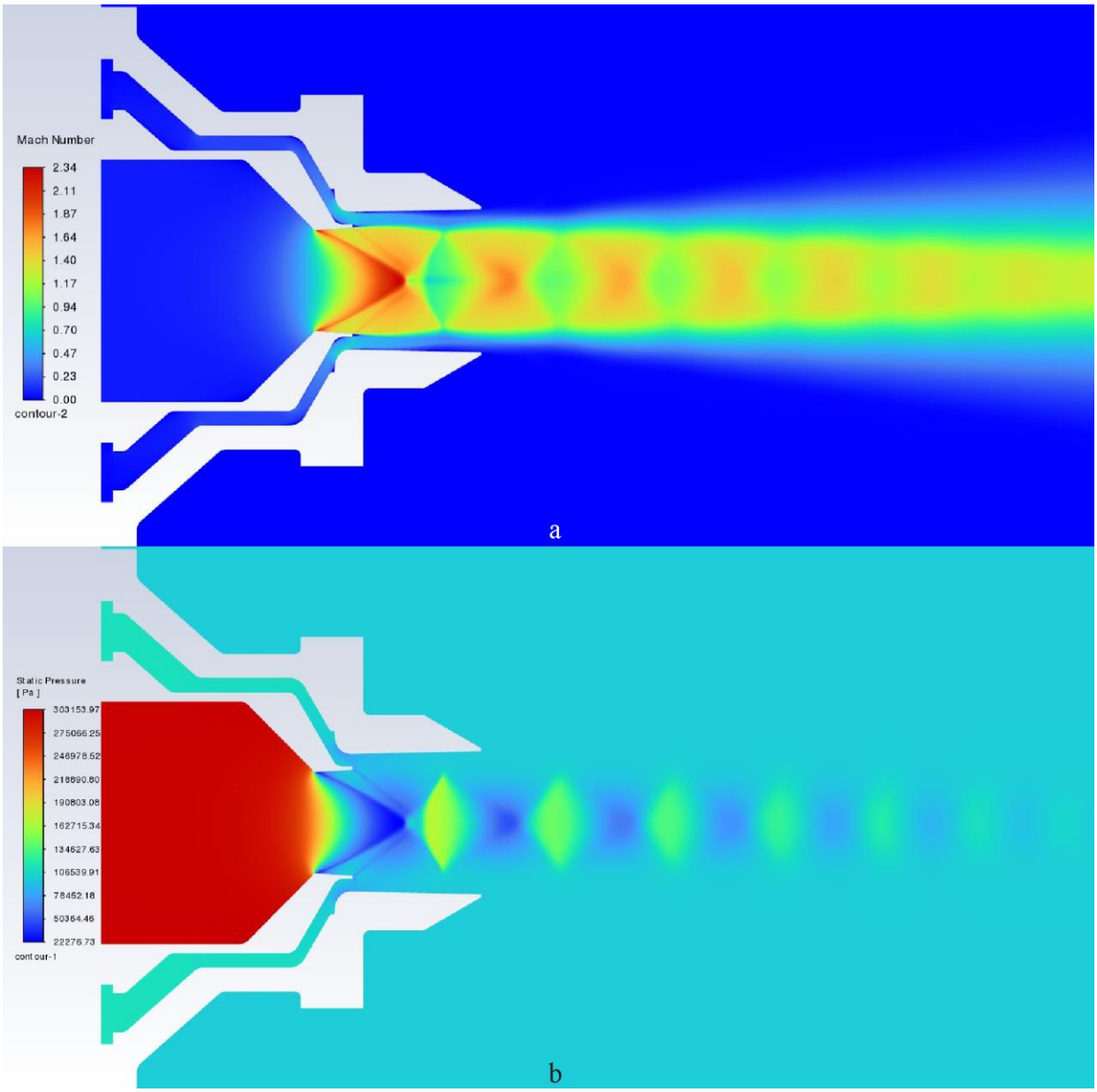

Fig. 10. Fields of Mach number (a) and static pressure (b) inside the considered ejector nozzle for k-ω (SST) turbulence model

Conclusions

1. It was not possible to find justification of choice of turbulence models for the CFD-analysis of thrust augmenting ejector nozzles within available literature.

2. Majority of authors of available researches, devoted to study of thrust augmenting ejector nozzle, use different versions of k-ε and k-ω turbulence models.

3. Digital data from NASA experiments [24] (which contain complete information about geometry, experimental static pressure distribution along the shroud of nozzles and their integral parameters and distinguishes with reliable data) has been selected for accuracy comparison of different turbulence models within this study. Axisymmetric model of the ejector nozzle has been constructed and boundary conditions have been set in accordance with data.

4. For mesh independence study, calculations in ANSYS Fluent 2024R1 have been conducted using three unstructured meshes having sizes of primary elements of 25, 12, and 6 mm and mesh improvement near nozzle walls to 0.5; 0.25 and 0.12 mm correspondingly. For estimation of uncertainty due to discretization, long established procedure using Grid Convergence Index – GCI has been used.

5. Mesh independence has been verified by means of comparison of calculation static pressure distribution along the inner wall of ejector nozzle shroud for three different meshes with experiment [24].

6. Accuracy of the calculation model has been validated by means of comparison of calculation integral parameters of ejector nozzle (thrust, average exit flow speed, and primary flow rate) with experimental ones [24].

7. Calculations with fourteen turbulence models were performed for the considered model of the ejector nozzle using medium mesh (with following application of adaptive mesh). Comparison of roof-mean-square and maximal deviations of calculation static pressure along the inner wall of the ejector nozzle shroud with their experimental values gave an opportunity to discover priority of these turbulence models by accuracy. Three turbulence models, which gave mistake of thrust calculation more than one per sent, have been rejected on the base of comparison of calculation integral parameters of ejector nozzle (thrust, average exit flow speed, and primary flow rate) with its experimental values.

8. On the base of multicriterion expert analysis of the obtained results, the best three models have been discovered: Spalart-Allmaras (Strain/Vorticity-Based), k-ω (BSL), k-ω (SST) and also seven models having acceptable level, which give mistakes of ejector nozzle thrust and primary flow rate calculation less than 1 %, and mistake of average flow speed at the ejector nozzle exit calculation, which does not exceed 5 %. Thus, just these models can be recommended for the following researches of thrust augmenting ejector nozzles.

Conflict of interest

The author declare that they have no conflict of interest in relation to this research, whether financial, personal, author ship or otherwise, that could affect the research and its results presented in this paper.

Financing

The study was performed without financial support.

Data availability

Manuscript has no associated data.

Use of artificial intelligence

The author confirm that they did not use artificial intelligence technologies when creating the current work.

All the author have read and agreed to the published version of this manuscript.

References

1. Schmidt, R., Hupfer, A., & Gümmer, V. *Experimental and Numerical Investigation of Mixer Ejector Nozzles for Small Turbojet Engines. Proceeding of ISABE 2022*, Ottawa, 25-30 September, 2022, pp. 1-14. Available at: https://www.researchgate.net/publication/372288860/ISABE_2021_036_full.pdf (accessed 28.02.2025).

2 Tsukanov, R., & Yepifanov, S. Review of Ejector Nozzles. Part 1 – Thrust Augmenting Ejector Nozzles. *Aviacijno-kosmicna tehnika i tehnologia – Aerospace technic and technology*, 2025, no. 4/204, pp. 45-59. DOI: 10.32620/aktt.2025.4.07.

3. Tsukanov, R., & Yepifanov, S. Review of Ejector Nozzles. Part 2 – Mixers and Additional Information. *Aviacijno-kosmicna tehnika i tehnologia – Aerospace technic and technology*, 2025, no. 4sup1/205, pp. 92-101. DOI: 10.32620/aktt.2025.4sup1.12.

4. Rushmore, W. L., & Zelazny, S. W. *A Three Dimensional Turbulent Compressible Flow Model for Ejector and Fluted Mixers: NASA Contractor Report CR-159467*, 1978. 133 p. Available at: https://ntrs.nasa.gov/api/citations/19790006154/downloads/19790006154.pdf (accessed 28.02.2025).

5. Speziale, C. G., Ridha, A., & Anderson, E. C. *A Critical Evaluation of Two-Equation Models for Near Wall Turbulence. NASA CR-182068*, 1990. 32 p. Available at: https://ntrs.nasa.gov/api/citations/19900016954/downloads/19900016954.pdf (accessed 30.01.2025).

6. DeBonis, J. R. *Full Navier-Stokes analysis of a two-dimensional mixer/ejector nozzle for noise suppres-*

ISSN 1814-4225 (print)
ISSN 2663-2012 (online)

sion. NASA Technical Memorandum AIAA-92-3570, 1992. 17 p. Available at: https://ntrs.nasa.gov/api/citations/19920017790/downloads/19920017790.pdf . (accessed 08.01.2025).

7. Jason, E. *Computational Study of Variable Area Ejector Rocket Flowfields*. 2004. 183 p. Available at: https://utoronto.scholaris.ca/server/api/core/ bitstreams/00261dd6-7ba9-420d-b2d5-b54c49df6aae/content. (accessed 08.01.2025).

8. Liu, Y.-H. Experimental and numerical research on high pumping performance mechanism of lobed exhauster-ejector mixer. *International Communications in Heat and Mass Transfer*. 2007, no. 34, pp. 197–209. DOI: 10.1016/j.icheatmasstransfer.2006.10.003.

9. Khalid, S., Sokhey, J., Chakka, P., & Pierluissi, A. Ejector/Engine/Nacelle Integration for Increased Thrust minus Drag. *Proceedings of the 46th AIAA/ASME/SAE/ASEE Joint Propulsion Conference & Exhibit*, Nashville, TN, USA, 25–28 July 2010. pp. 1-11. DOI: 10.2514/6.2010-6501.

10. Thirumurthy, D., Blaisdell, G., Lyrintzis, A., & Sullivan, J. Preliminary design and computational analysis of an ejector nozzle with chevrons. *Proceeding of 49th AIAA Aerospace Sciences Meeting including the New Horizons Forum and Aerospace Exposition*, Orlando, Florida, 2011, pp. 1-17. Available at: https://doi.org/10.2514/6.2011-918 (accessed 28.02.2025).

11. Luginsland, T. How the nozzle geometry impacts vortex breakdown in compressible swirling-jet flows. *AIAA Journal*, 2015. vol. 53, iss. 10, pp. 1–15. DOI: 10.2514/1.J053843.

12. Hoter, Z., Castner, R. S., & Zaman, K. Q. CFD Optimization of Ejector Flaps in a One-Sided Mixer Ejector Nozzle. *In Proceedings of the AIAA Scitech 2019 Forum*, San Diego, CA, USA, 7–11 January 2019. pp. 1-12. DOI: 10.2514/6.2019-0544.

13. Dong, Z., Sun, M., Wang, Z., Cai, Z., Yao, Y., & Gu, R. Numerical investigation on flow and mixing characteristics inside a converging-diverging mixing duct of rocket-based combined-cycle engine in ejector mode. *Aerosp. Sci. Technol.* 2020, vol. 106, pp. 1-15. DOI: 10.1016/j.ast.2020.106102.

14. Huang, H., Zhang, K., Tan, H., Lu, S., Zhao, L., Lei, M., & Ling, W. Flow Characteristics of an Integrated Ejector Nozzle with Tertiary Intake. *Journal of Propulsion Technology*. 2020, vol. 41, no. 12, pp. 2729–2738. DOI: 10.13675/j.cnki.tjjs.200170.

15. Li, H., Wang, X., Ning, J., Zhang, P., Hu, H., & Tu, J. Numerical Investigation of the nozzle expansion state and its effect on the performance of the steam ejector based on ideal gas model. *Applied Thermal Engineering*. 2021, vol. 199, pp. 1-32. DOI: 10.1016/j.applthermaleng.2021.117509.

16. Li, Z., & Wang, H. Comparison of the Flow Fields between Nozzles with Full-Open and Open-Close Valves at Transonic Velocity. *Hindawi Journal of Applied Mathematics*, 2022, article no. 6875240, pp. 1-11. DOI: 10.1155/2022/6875240.

17. Li, Z., Wang, H., & Huang, H. Analysis of Flow Field of Three-Dimensional Ejector Nozzle with Open-close Alternate Intake Valve at Transonic Velocity. *Journal of Aerospace Power*, 2023, vol. 38, no. 12, pp. 2937–2947. DOI: 10.13224/j.cnki.jasp.20210581.

18. Li, Z., & Wang, H. Flow characteristics of ejector nozzles with different auxiliary intake valves. *AIP Advances*, 2024, vol. 14, article no. 015237. pp. 1-9. DOI: 10.1063/5.0187268.

19. Nwoye, F. C., Okoro, H., Okoronkwo, C., Nwaji, G., Nwufo, O., & Emmanuel, A. Changes in Primary Nozzle Contours and Ejector Performance – A Numerical Study. *International Journal of Advantage Scientific Engineering*, 2024, vol. 10, no.3 pp. 3495-3507. DOI: 10.29294/IJASE.10.3.2024.3495-3507.

20. Vinz, A., & Raichle, A. Investigation of the effects of boundary layer ingestion engine integration on aircraft thrust requirement. *CEAS Aeronautical Journal*, 2024, vol. 15, pp. 1235-1250. DOI: 10.1007/s13272-024-00722-0.

21. He, Y., Shi, X., & Ji, H. Optimal Design of Ejector Nozzle Profile with Internal and External Integrated Flow. *Aerospace*, 2024, vol. 11, iss. 3, article no. 184. pp. 1-17. DOI: 10.3390/aerospace11030184.

22. Bellary, S. A. I., Dabir, S. A., Khan, S. A., Tamhane, T., Shaikh, J. H., & Khan, A. Computational Analysis of Thrust Generated by Converging Diverging Nozzle at Different Diverging Angle. *Journal of Advanced Research in Numerical Heat Transfer*, 2025, vol. 29, iss. 1, pp. 102-128. DOI: 10.37934/arnht.29.1.102128.

23. Scarlatella, G., Sieder-Katzmann, J., Propst, M., Heutling, T., Petersen, J., Weber, F., Portolani, M., Garutti, M., Bianchi, D., Pastrone, D., Ferrero, A., Tajmar, M., & Bach, C. RANS Simulations of Advanced Nozzle Performance and Retro-Flow Interactions for Vertical Landing of Reusable Launch Vehicles. *Aerospace*, 2025, vol. 12, iss. 124. pp. 1-30. DOI: 10.3390/aerospace12020124.

24. Lamb, M. *Internal Performance Characteristics of Thrust-Vectored Axisymmetric Ejector Nozzles*: NASA Technical Memorandum NASA-TM-4610, 1998. 232 p. Available at: https://ntrs.nasa.gov/api/citations/19950018918/downloads/19950018918.pdf . (accessed 08.01.2025).

25. Celik, I. B., Ghia, U., Roache, P. J., Freitas, C. J., Coleman, H., & Raad, P. E. Procedure for Estimation and Reporting of Uncertainty Due to Discretization in CFD Applications. *Journal of Fluids En-*

gineering, 2008, vol. 130, pp. 1-4. DOI: 10.1115/1.2960953.

26. Teschner, T.-R. *How to Manage Uncertainty in CFD: the Grid Convergence Index*. 2025. 36 p. Available at: https://cfd.university/blog/how-to-manage-uncertainty-in-cfd-the-grid-convergence-index. (accessd 11.09.2025).

27. Saaty, T. L. *The Analytic Hierarchy Process: Planning, Priority Setting, Resource Allocation*. New York, McGraw-Hill, 1980. 287 p.

Received 18.12.2025, Received in revised form 05.01.2025
Accepted date 19.01.2026, Published date 22.01.2026

ПОРІВНЯННЯ РІЗНИХ МОДЕЛЕЙ ТУРБУЛЕНТНОСТІ ДЛЯ ДОСЛІДЖЕННЯ ЕЖЕКТОРНИХ СОПЕЛ МЕТОДОМ ОБЧИСЛЮВАЛЬНОЇ ГІДРОДИНАМІКИ

Р. Ю. Цуканов

Предметом вивчення в статті є різні моделі турбулентності у застосуванні до розрахунків ежекторних сопел, призначених для підвищення тяги реактивних двигунів, методом обчислювальної гідродинаміки. **Метою** є обґрунтування вибору моделі турбулентності для таких задач. **Задачі:** пошук і аналіз літературних джерел щодо використання різних моделей турбулентності в CFD-розрахунках ежекторних сопел для підвищення тяги; вибір надійного й повного джерела експериментальних даних для числового моделювання; побудова вісесиметричної моделі ежекторного сопла і трьох сіток (грубої, середньої й тонкої); задання граничних умов; оцінювання помилки дискретизації з використанням індексу сіткової збіжності – Grid Convergence Index – GCI; підтвердження сіткової незалежності; підтвердження точності розрахункової моделі; розрахунки з використанням чотирнадцяти моделей турбулентності; виявлення пріоритету точності цих моделей турбулентності; формулювання рекомендацій щодо використання моделей турбулентності для таких задач. Використовуваними **методами є:** пошук відповідних джерел у мережі Internet та їх аналіз виходячи з власного досвіду роботи в авіаційній галузі; метод обчислювальної гідродинаміки; числові розрахунки індексу сіткової збіжності й аналіз похибок. Отримано наступні **результати.** На основі знайдених джерел інформації виявлено, що більшість авторів наявних досліджень, присвячених дослідженню ежекторних сопел для підвищення тяги, використовує різні версії моделей турбулентності k-ε та k-ω. На основі даних з меморандуму NASA побудовано розрахункову модель ежекторного сопла та трьома різними способами (з використанням GCI, порівнянням розподілу статичного тиску по обичайці сопла та порівнянням інтегральних параметрів сопла) підтверджено її точність. На основі цієї моделі ежекторного сопла виконано розрахунки з використанням чотирнадцяти моделей турбулентності та шляхом порівняння з експериментальними даними NASA і багатокритеріального експертного аналізу отриманих результатів виявлено три найкращі моделі турбулентності, що дають найменші похибки (розподілу статичного тиску по обичайці сопла та розрахунку інтегральних параметрів сопла). **Висновки.** Наукова новизна отриманих результатів полягає в наступному: на підставі порівняння результатів числового моделювання ежекторного сопла з використанням чотирнадцяти моделей турбулентності з експериментальними даними NASA виявлено три моделі турбулентності, що дають найменші похибки, які можна рекомендувати для розрахунків ежекторних сопел для підвищення тяги. Таким чином виявлено моделі турбулентності, які можна використовувати для розроблення методики проєктування ежекторного сопла для підвищення тяги мікро-турбореактивних двигунів. Намічено мету та задачі подальших досліджень у цій галузі.

Ключові слова: ежекторне сопло для підвищення тяги; тяга сопла; індекс сіткової збіжності; моделі турбулентності; похибка спричинена дискретизацією; розподіл тиску по обичайці.

Цуканов Руслан Юрійович – старш. викл. каф. проектування літаків і вертольотів, Національний аерокосмічний університет «Харківській авіаційний інститут», Харків, Україна.

Ruslan Tsukanov – Senior Lecturer at the Airplane and Helicopter Design Department, National Aerospace University «Kharkiv Aviation Institute», Kharkiv, Ukraine,
e-mail: r.tsukanov@khai.edu, ORCID: 0000-0001-8348-8707, Scopus ID: 57486195800.